Inorg. Chem. **2002**, *41*, 2134–2145

Intercalated Organic–Inorganic Perovskites Stabilized by Fluoroaryl–Aryl Interactions

David B. Mitzi,* David R. Medeiros, and Patrick R. L. Malenfant†

IBM T. J. Watson Research Center, P.O. Box 218, Yorktown Heights, New York 10598

Received November 21, 2001

Crystals of several new hybrid tin(II) iodide-based perovskites, involving 2,3,4,5,6- pentafluorophenethylammonium or phenethylammonium cation bilayers and intercalated aryl or perfluoroaryl molecules, were grown by slow evaporation of a methanol solution containing the hybrid perovskite and the intercalating species. The $(C_6F_5C_2H_4NH_3)_2SnI_4\cdot(C_6H_6)$ structure was solved at –75 °C in a monoclinic *C*2/*c* subcell [$a = 41.089(12)$ Å, $b = 6.134(2)$ Å, $c = 12.245(3)$ Å, $\beta = 94.021(5)°$, $Z = 4$] and consists of sheets of corner-sharing distorted SnI_6 octahedra separated by bilayers of pentafluorophenethylammonium cations. The intercalated benzene molecules form a single well-ordered layer interposed between adjacent fluoroaryl cation layers. The corresponding hybrid with an unfluorinated organic cation and fluorinated intercalating molecule, $(C_6H_5C_2H_4NH_3)_2SnI_4\cdot(C_6F_6)$, is isostructural [$a = 40.685(4)$ Å, $b = 6.0804(6)$ Å, $c = 12.163(1)$ Å, $\beta = 93.136(2)°$, $Z = 4$]. For each intercalated system, close C···C contacts (3.44–3.50 Å) between the aromatic cation and the intercalated molecule are indicative of a significant face-to-face interaction, similar to that found in the complex $C_6H_6\cdot C_6F_6$. Crystal growth runs with the organic cation and prospective intercalating molecule either both fluorinated or both unfluorinated did not yield stable intercalated compounds, demonstrating the significance of fluoroaryl–aryl interactions in the current intercalated structures. Thermal analysis of $(C_6F_5C_2H_4NH_3)_2SnI_4\cdot(C_6H_6)$ and $(C_6H_5C_2H_4NH_3)_2SnI_4\cdot(C_6F_6)$ crystals yields, in addition to the characteristic transitions of the parent perovskite, endothermic transitions [12.6(5) and 32.1(8) kJ/mol, respectively] with an onset at 145 °C and a weight loss corresponding to the complete loss of the intercalated molecule. The relatively high deintercalation temperature (well above the boiling point of benzene and hexafluorobenzene) demonstrates the usefulness of the hybrid perovskites in providing a stable framework for the examination of the fluoroaryl–aryl interaction, as well as the potential importance of this interaction in tailoring new hybrid perovskites. UV–vis absorption measurements on $(C_6H_5C_2H_4NH_3)_2SnI_4\cdot(C_6F_6)$ thin films indicate a small reversible wavelength shift to higher energy for the tin(II) iodide framework exciton peak (with respect to that of the parent perovskite spectrum), from 608(2) nm [2.04 eV] to 595(2) nm [2.08 eV], and a corresponding shift in the band edge position. This spectral shift can most reasonably be attributed to subtle structural changes induced in the tin(II) iodide sheets by the intercalated hexafluorobenzene molecules.

Introduction

Organic−inorganic perovskites provide a range of important opportunities for the examination of structural templating[1,2] and the design of multifunctional materials.[3−6] Interesting properties within the hybrid perovskites include a semiconductor−metal transition,[7,8] strong fluorescence,[9−11] a nonlinear optical response,[12,13] magnetic transitions,[14−16] and tunable polariton absorption.[17] Recently, the flexible chemical nature of the hybrids has enabled the design of an organic−inorganic light-emitting device (OILED) based on a dye-containing organic−inorganic perovskite.[18] An organic−

* To whom correspondence should be addressed. E-mail: dmitzi@us.ibm.com.

† Current address: Polymeric Materials Laboratory, General Electric Co., K1-4A49, 1 Research Circle, Niskayuna, NY 12309.

(1) Mitzi, D. B. *J. Chem. Soc., Dalton Trans.* **2001**, 1.
(2) Mitzi, D. B. *Inorg. Chem.* **2000**, *39*, 6107.
(3) Day, P.; Ledsham, R. D. *Mol. Cryst. Liq. Cryst.* **1982**, *86*, 163.
(4) Mitzi, D. B. *Prog. Inorg. Chem.* **1999**, *48*, 1.
(5) Mitzi, D. B.; Chondroudis, K.; Kagan, C. R. *IBM J. Res. Dev.* **2001**, *45*, 29.
(6) Mitzi, D. B.; Chondroudis, K.; Kagan, C. R. *Inorg. Chem.* **1999**, *38*, 6246.
(7) Mitzi, D. B.; Feild, C. A.; Harrison, W. T. A.; Guloy, A. M. *Nature* **1994**, *369*, 467.
(8) Mitzi, D. B.; Wang, S.; Feild, C. A.; Chess, C. A.; Guloy, A. M. *Science* **1995**, *267*, 1473.
(9) Papavassiliou, G. C.; Koutselas, I. B. *Synth. Met.* **1995**, *71*, 1713.

10.1021/ic011190x CCC: $22.00
Published on Web 03/27/2002

inorganic field-effect transistor (OIFET) has also been demonstrated,[19−21] with a solution-processed perovskite channel layer and a mobility comparable to that found in amorphous silicon devices. The hybrid devices and interesting physical properties highlight the ability to combine useful attributes of organic and inorganic materials within the perovskite structure.

The basic perovskite structure consists of layers of corner-sharing metal halide octahedra alternating with bilayers of organic cations (generally a protonated organic ammonium species). Many of the interesting properties of the hybrid perovskites arise predominantly in the inorganic component of the structure. In the reported conducting tin(II) iodide-based perovskites, for example, electrical transport arises in the inorganic framework.[7,8] In lead(II), tin(II), and germanium(II) halide perovskites with relatively simple organic cation layers (i.e., those with a large HOMO−LUMO energy gap), strong photoluminescence in the visible spectral range arises from the radiative decay of excitons associated with the band gap of the inorganic sheets.[9−11] The organic layers play a secondary role in the luminescence by making the structure more two-dimensional and by providing a lower dielectric constant layer around the inorganic sheets (thereby reducing the screening and increasing the Coulomb interaction that binds the electron−hole pair).[22]

Recently more interest has focused on the organic component of the hybrid. While most examples of the layered perovskites contain relatively simple organic cations (e.g., alkylammonium and single-ring aromatic cations), more complex organic molecules can also be incorporated subject to certain chemical and structural constraints.[1] In hybrid perovskites containing the oligothiophene derivative 5,5‴-bis(aminoethyl)-2,2′:5′,2″:5″,2‴-quaterthiophene[6] or the pyrene derivative 1-pyrenemethylamine,[23] luminescence arising from the organic molecule is substantially dependent on the inorganic framework, demonstrating interaction between the two components of the structure. Topochemical solid-state polymerization of the organic cation layer has also been reported for hybrids containing photosensitive organic cations.[3,24,25] In this case, the inorganic framework acts as a template, controlling whether the potentially photoreactive molecule will be held in a configuration appropriate for polymerization. Finally, hybrid systems containing long-chain alkylammonium cations allow for the study of structural transitions within lipid bilayers.[26]

Another interesting degree of flexibility within the organic component of the hybrid perovskite family, which has not been widely considered, is the possibility of intercalating functional molecules within the van der Waals gap of the organic bilayer. Intercalated systems have numerous interesting prospective properties, including superconductivity,[27] ionic conductivity,[28] and photofunctionality (e.g., photocatalysis, photoinduced charge separation, photoluminescence, photochromism, and nonlinear optical properties).[29] Dolzhenko et al.[30] have reported the intercalation of weakly interacting molecules (1-chloronaphthalene, *o*-dichlorobenzene, and hexane) into lead(II) iodide- and cadmium(II) chloride-based perovskites with long-chain aliphatic cations. Given the weak van der Waals interaction between the organic cation and the intercalating species, however, the intercalated molecules quickly deintercalate from single crystals, making it difficult to study the composite systems over extended periods of time. Furthermore, it has been proposed that the observed changes reported in powder diffraction patterns for the lead(II) iodide-based systems may result from a structural change brought about by the endothermic evaporation of the solvent (i.e., hexane) rather than from an intercalation process.[31] In an effort to unambiguously demonstrate and further stabilize intercalated hybrid perovskite systems at room temperature, we considered the design of systems with enhanced interaction between the intercalated species and the van der Waals gallery into which the organic species must fit.

Noncovalent interactions between aromatic groups have been shown to play a significant role in the design and structural organization of chemical and biological systems.[32−34] One such example, fluoroaryl−aryl interaction, is responsible for the anomalously high melting temperature (23.7 °C) of the 1:1 complex formed between benzene and hexafluorobenzene (with individual melting points of 5.4 and 5.0 °C, respectively).[35] The face-to-face stacking and interaction within the complex is believed to be primarily electrostatic in origin (as a result of the relatively large, but opposite in

(10) Ishihara, T.; Takahashi, J.; Goto, T. *Phys. Rev. B* **1990**, *42*, 11099.
(11) Mitzi, D. B. *Chem. Mater.* **1996**, *8*, 791.
(12) Calabrese, J.; Jones, N. L.; Harlow, R. L.; Herron, N.; Thorn, D. L.; Wang, Y. *J. Am. Chem. Soc.* **1991**, *113*, 2328.
(13) Xu, C.; Kondo, T.; Sakakura, H.; Kumata, K.; Takahashi, Y.; Ito, R. *Solid State Commun.* **1991**, *79*, 245.
(14) de Jongh, L. J.; Botterman, A. C.; de Boer, F. R.; Miedema, A. R. *J. Appl. Phys.* **1969**, *40*, 1363.
(15) Willett, R.; Place, H.; Middleton, M. *J. Am. Chem. Soc.* **1988**, *110*, 8639.
(16) Sekine, T.; Okuno, T.; Awaga, K. *Inorg. Chem.* **1998**, *37*, 2129.
(17) Fujita, T.; Sato, Y.; Kuitani, T.; Ishihara, T. *Phys. Rev. B* **1998**, *57*, 12428.
(18) Chondroudis, K.; Mitzi, D. B. *Chem. Mater.* **1999**, *11*, 3028.
(19) (a) Chondroudis, K.; Dimitrakopoulos, C. D.; Mitzi, D. B. Unpublished work, 1998. (b) Chondroudis, K.; Dimitrakopoulos, C. D.; Kagan, C. R.; Kymissis, I.; Mitzi, D. B. United States Patent US6,180,956, Jan 30, 2001.
(20) Kagan, C. R.; Mitzi, D. B.; Dimitrakopoulos, C. D. *Science* **1999**, *286*, 945.
(21) Mitzi, D. B.; Dimitrakopoulos, C. D.; Kosbar, L. L. *Chem. Mater.* **2001**, *13*, 3728.
(22) Hong, X.; Ishihara, T.; Nurmikko, A. V. *Phys. Rev. B* **1992**, *45*, 6961.
(23) Braun, M.; Tuffentsammer, W.; Wachtel, H.; Wolf, H. C. *Chem. Phys. Lett.* **1999**, *307*, 373.
(24) Tieke, B.; Chapuis, G. *Mol. Cryst. Liq. Cryst.* **1986**, *137*, 101.
(25) Tieke, B.; Wegner, G. *Makromol. Chem., Rapid Commun.* **1981**, *2*, 543.
(26) Needham, G. F.; Willett, R. D.; Franzen, H. F. *J. Phys. Chem.* **1984**, *88*, 674.
(27) Gamble, F. R.; Osiecki, J. H.; Cais, M.; Pisharody, R.; DiSalvo, F. J.; Geballe, T. H. *Science* **1971**, *174*, 493.
(28) Clearfield, A. *Chem. Rev.* **1988**, *88*, 125.
(29) Ogawa, M.; Kuroda, K. *Chem. Rev.* **1995**, *95*, 399.
(30) Dolzhenko, Y. I.; Inabe, T.; Maruyama, Y. *Bull. Chem. Soc. Jpn.* **1986**, *59*, 563.
(31) Ishihara, T. In *Optical Properties of Low-Dimensional Materials*; Ogawa, T., Kanemitsu, Y., Eds.; World Scientific: Singapore, 1995; pp 288−339.
(32) Burley, S. K.; Petsko, G. A. *Science* **1985**, *229*, 23.
(33) (a) Cubberley, M. S.; Iverson, B. L. *J. Am. Chem. Soc.* **2001**, *123*, 7560. (b) Seel, C.; Vögtle, F. *Angew. Chem., Int. Ed. Engl.* **1992**, *31*, 528.
(34) Hunter, C. A. *Chem. Soc. Rev.* **1994**, *23*, 101.
(35) Patrick, C. R.; Prosser, G. S. *Nature* **1960**, *187*, 1021.

sign, quadrupole moments of C_6H_6 and C_6F_6),[36] and has been shown to be a more general supramolecular motif within structurally engineered materials.[37] The fluoroaryl−aryl interaction has been used to order molecular systems for photochemically induced topochemical [2 + 2] reactions in the solid state,[38] as well as for the control of liquid crystal phase behavior,[39] and the self-organization of J aggregates for optoelectronic applications.[40] In this study, the first two examples of intercalated hybrid perovskite systems stabilized by fluoroaryl−aryl interactions are presented. The substantial stability of the intercalated perovskites enables a full consideration of crystallographic, thermal, and optical properties of the systems and therefore a closer examination of the important fluoroaryl−aryl interaction in solids. The resulting structures demonstrate that fluoroaryl−aryl interaction is a new means of tailoring the structural chemistry and properties of the hybrid perovskites.

Experimental Section

Synthesis. $(C_6F_5C_2H_4NH_3)_2SnI_4$·Benzene. Crystals of the intercalated material $(C_6F_5C_2H_4NH_3)_2SnI_4$·$(C_6H_6)$, based on the 2,3,4,5,6-pentafluorophenethylammonium cation, were grown by slowly evaporating a methanol/benzene solution of the $(C_6F_5C_2H_4NH_3)_2SnI_4$ perovskite. First, 42.0 mg (0.04 mmol) of $(C_6F_5C_2H_4NH_3)_2SnI_4$ crystals [prepared as described previously for other fluorophenethylammonium tin(II) iodide crystals,[21] using 2,3,4,5,6-pentafluorophenethylamine[41] as the base for the organic salt] were added to a vial under an argon atmosphere along with 0.5 mL of anhydrous methanol, leading to the dissolution of the crystals. An excess of anhydrous benzene (2 mL) was added to the solution, and the vial was agitated to produce a homogeneous, light yellow solution. After the loosely covered vial was allowed to sit in an inert atmosphere for several days (to allow for evaporation of a portion of the solvent), red, platelike crystals of the benzene-intercalated perovskite formed. Anal. Calcd for the unintercalated $(C_6F_5C_2H_4NH_3)_2SnI_4$ starting material: C, 18.29; H, 1.34; N, 2.67. Found: C, 18.4; H, 1.3; N, 2.6. Anal. Calcd for the intercalated $(C_6F_5C_2H_4NH_3)_2SnI_4$·$(C_6H_6)$ material: C, 23.41; H, 1.79; N, 2.48. Found: C, 23.0; H, 1.9; N, 2.4.

$(C_6H_5C_2H_4NH_3)_2SnI_4$·Hexafluorobenzene. $(C_6H_5C_2H_4NH_3)_2SnI_4$·$(C_6F_6)$ crystals were grown using a process essentially identical to that described above for the $(C_6F_5C_2H_4NH_3)_2SnI_4$·$(C_6H_6)$ analogue. First, 34.8 mg (0.04 mmol) of $(C_6H_5C_2H_4NH_3)_2SnI_4$ crystals [prepared as described previously for fluorophenethylammonium tin(II) iodide crystals, using phenethylamine as the base for the organic salt][21] were added to a vial under an argon atmosphere along with 1.0 mL of anhydrous methanol, leading to the dissolution of the crystals. An excess of anhydrous hexafluorobenzene (1 mL) was added to the solution, and the vial was agitated to produce a homogeneous, light yellow solution. After the loosely covered vial was allowed to sit in an inert atmosphere for several days, red, platelike crystals of the hexafluorobenzene-intercalated perovskite were formed. Anal. Calcd for the unintercalated $(C_6H_5C_2H_4NH_3)_2SnI_4$ starting material: C, 22.07; H, 2.78; N, 3.22. Found: C, 22.0; H, 2.9; N, 3.1. Anal. Calcd for the intercalated $(C_6H_5C_2H_4NH_3)_2SnI_4$·$(C_6F_6)$ material: C, 25.00; H, 2.29; N, 2.65. Found: C, 24.9; H, 2.5; N, 2.5.

Thin Film Deposition. Films of the unintercalated tin(II) iodide perovskites were prepared in a nitrogen-filled drybox by spin-coating from solution. The quartz substrates for optical measurements were cleaned by room-temperature sonication in toluene (20 min), acetone (20 min), and methanol (20 min). They were subsequently placed in a 110 °C oven to dry. The spinning solutions for each compound were prepared by dissolving 40 mg of recrystallized perovskite in 0.6 mL of freshly dried and distilled methanol. The films were prepared by flooding the surface of the substrate with solution (filtered through a 0.2 μm poly(tetrafluoroethylene) filter) and then initiating a spinning cycle (1 s ramp to 1800 rpm; dwell 30 s at 1800 rpm). Each substrate was annealed at 70 °C for 15 min after being spun to remove residual solvent. The films exhibited at least 7 orders of well-defined X-ray diffraction peaks corresponding to the (2*h*, 0, 0) series of reflections [refined *d* spacings for these series of reflections are 35.0(1) Å for $(C_6F_5C_2H_4NH_3)_2SnI_4$ and 32.6(1) Å for $(C_6H_5C_2H_4NH_3)_2SnI_4$], indicating that the films were well crystallized and highly oriented.

Films of $(C_6F_5C_2H_4NH_3)_2SnI_4$·$(C_6H_6)$ were prepared by immersing the unintercalated films in a room-temperature benzene solution for approximately 60 min. Given the thin nature of the films (~300 Å), deintercalation proceeded much more rapidly than in the single-crystal samples. The films were therefore crudely encapsulated by placing a thin (5 μm) polycarbonate sheet on top while they were still wet from the benzene solution. The interaction of the polycarbonate sheet with the benzene and organic−inorganic hybrid effectively laminates the sheet to the hybrid film, thereby providing a partial diffusion barrier for the intercalated species and lengthening the amount of time available for the measurements before deintercalation. Both X-ray diffraction measurements and optical measurements (at wavelengths longer than 300 nm) could be made through the thin polycarbonate sheet and were performed immediately after the intercalation process to minimize intercalant loss. Films of $(C_6H_5C_2H_4NH_3)_2SnI_4$·$(C_6F_6)$ were prepared similarly, by immersing the unintercalated films in a 60 °C hexafluorobenzene solution for approximately 60 min. A polycarbonate sheet was used to maintain a thin layer of hexafluorobenzene trapped between the sheet and the surface of the film during measurement. The intercalated films exhibited well-defined X-ray diffraction peaks, again corresponding to the (2*h*, 0, 0) series of reflections [refined *d* spacings for these series of reflections are 41.4(1) Å for $(C_6F_5C_2H_4NH_3)_2SnI_4$·$(C_6H_6)$ and 41.2(1) Å for $(C_6H_5C_2H_4NH_3)_2SnI_4$·$(C_6F_6)$].

X-ray Crystallography. A red $(C_6F_5C_2H_4NH_3)_2SnI_4$·$(C_6H_6)$ [$(C_6H_5C_2H_4NH_3)_2SnI_4$·$(C_6F_6)$] platelike crystal, with the approximate dimensions 0.02 mm × 0.20 mm × 0.62 mm [0.05 mm × 0.07 mm × 0.20 mm], was selected under a microscope and attached to the end of a quartz fiber with 5 min epoxy. Despite the relative stability of the crystals at room temperature, low-temperature data collection was employed to reduce thermal parameters and to facilitate locating the intercalated species in the difference maps. A full sphere of data was collected at −75 °C on a Bruker SMART CCD diffractometer, equipped with a normal focus 2.4 kW sealed tube X-ray source (Mo Kα radiation). Intensity data were collected with a detector distance of approximately 5.0 cm, in 2272 frames with increasing ω, and an exposure time of 60 s [120 s] per frame. The increment in ω between each frame was 0.3°.

(36) (a) Brown, N. M. D.; Swinton, F. L. *Chem. Commun.* **1974**, 770. (b) Williams, J. H. *Acc. Chem. Res.* **1993**, *26*, 593.
(37) Coates, G. W.; Dunn, A. R.; Henling, L. M.; Dougherty, D. A.; Grubbs, R. H. *Angew. Chem., Int. Ed. Engl.* **1997**, *36*, 248.
(38) Coates, G. W.; Dunn, A. R.; Henling, L. M.; Ziller, J. W.; Lobkovsky, E. B.; Grubbs, R. H. *J. Am. Chem. Soc.* **1998**, *120*, 3641.
(39) Dai, C.; Nguyen, P.; Marder, T. B.; Scott, A. J.; Clegg, W.; Viney, C. *Chem. Commun.* **1999**, 2493.
(40) Feast, W. J.; Lövenich, P. W.; Puschmann, H.; Taliani, C. *Chem. Commun.* **2001**, 505.
(41) Filler, R.; Chen, W.; Woods, S. M. *J. Fluorine Chem.* **1995**, *73*, 95.

Table 1. Crystallographic Data for $(C_6F_5C_2H_4NH_3)_2SnI_4\cdot(C_6H_6)$ and $(C_6H_5C_2H_4NH_3)_2SnI_4\cdot(C_6F_6)$

chemical formula	$(C_6F_5C_2H_4NH_3)_2SnI_4\cdot(C_6H_6)$	$(C_6H_5C_2H_4NH_3)_2SnI_4\cdot(C_6F_6)$
fw	1128.73	1056.76
space group	*C*2/*c* (no. 15)	*C*2/*c* (no. 15)
a, Å	41.089(12)	40.685(4)
b, Å	6.134(2)	6.0804(6)
c, Å	12.245(3)	12.163(1)
β, deg	94.021(5)	93.136(2)
V, Å^3	3079(1)	3004.5(5)
Z	4	4
ρ_{calcd}, g/cm^3	2.435	2.336
wavelength, Å	0.71073 (Mo Kα)	0.71073 (Mo Kα)
abs coeff (μ), cm^{-1}	49.2	50.1
R_f[a]	0.041	0.042
R_w[b]	0.053	0.054
goodness of fit (GoF)[c]	2.22	2.08

[a] $R_f = \sum(|F_o| - |F_c|)/\sum(|F_o|)$. [b] $R_w = \{\sum w(|F_o| - |F_c|)^2/\sum(w|F_o|^2)\}^{1/2}$. [c] GoF $= \{\sum w(|F_o| - |F_c|)^2/(n - m)\}^{1/2}$, where n = number of reflections and m = number of refinement parameters.

For the $(C_6F_5C_2H_4NH_3)_2SnI_4\cdot(C_6H_6)$ and $(C_6H_5C_2H_4NH_3)_2SnI_4\cdot(C_6F_6)$ compounds, examination of the CCD frames indicated the existence of two types of reflections. One set consisted of sharp, strong, well-defined peaks arising from subcells with the triclinic lattice parameters $a = 6.134(2)$ Å, $b = 12.243(5)$ Å, $c = 20.775(9)$ Å, $\alpha = 94.03(1)°$, $\beta = 98.49(1)°$, and $\gamma = 89.92(1)°$, and $a = 6.076(2)$ Å, $b = 12.155(4)$ Å, $c = 20.557(7)$ Å, $\alpha = 93.10(1)°$, $\beta = 98.50(1)°$, and $\gamma = 89.98(1)°$, respectively. These primitive cells were transformed to the C-centered monoclinic cells shown in Table 1. For the $(C_6H_5C_2H_4NH_3)_2SnI_4\cdot(C_6F_6)$ structure, a second set of more diffuse spots (broader and/or with a large background) doubled the initial triclinic subcell along the *a* axis. The Bravais lattice for the larger cell, which includes the diffuse reflections, is primitive triclinic. Similar diffuse reflections are observed for the $(C_6F_5C_2H_4NH_3)_2SnI_4\cdot(C_6H_6)$ crystal. While the structures can be solved in the larger triclinic cells, the *R* factors are substantially larger than for the refinements in the subcells with several large residual peaks in the inorganic layer of the refined structure, indicating that the ordering giving rise to the superstructure of the larger cell is not perfect or that there is a further unresolved superstructure. Therefore, in the current study, only the subcell structure is reported.

The final subcell parameters (Table 1) and crystal orientation matrix were obtained by a least-squares fit of 4399 [6714] reflections. An empirical absorption correction based on equivalent reflections was applied to the intensity data.[42] The structure was solved and refined using the NRCVAX 386 PC version program.[43] First, the Sn and I atoms were located using direct methods. The F, N, and C atoms were then located using successive Fourier difference maps. All heavy atoms (Sn, I, C, N, and F) were refined anisotropically. The hydrogen atoms on the terminal ammonium and adjacent methylene group of each organic cation could not be located in the difference maps. All other hydrogen atoms were located and refined isotropically. Attempts to refine the occupancy of the intercalating species component atoms led to results close to unity [e.g., for the hexafluorobenzene molecule in $(C_6H_5C_2H_4NH_3)_2SnI_4\cdot(C_6F_6)$, the occupancies all refined within the range 1.01−1.06]. Consequently, these values were fixed at 1. The minimum and maximum peaks in the final difference Fourier maps corresponded to −1.60 and 1.51 e/Å^3 [−1.32 and 1.30 e/Å^3]. No additional symmetry was detected for either of the compounds using the MISSYM program.[44] Selected crystallographic results for the two compounds are summarized in Table 1. The atomic coordinates for $(C_6F_5C_2H_4NH_3)_2SnI_4\cdot(C_6H_6)$ and $(C_6H_5C_2H_4NH_3)_2SnI_4\cdot(C_6F_6)$ are listed in Tables 2 and 3, respectively. Selected bond distances and angles are provided for each compound in Tables 4 and 5. A complete listing of crystallographic data, along with anisotropic displacement parameters for each compound, is given as Supporting Information.

Table 2. Positional and Thermal Parameters[a] for $(C_6F_5C_2H_4NH_3)_2SnI_4\cdot(C_6H_6)$

atom	x	y	z	B_{iso} (Å^2)
Sn	0.5	0.00958(6)	0.25	2.53(2)
I(1)	0.42279(1)	0.01510(5)	0.22725(2)	2.45(1)
I(2)[b]	0.50069(1)	0.1281(1)	0.00453(4)	2.03(2)
I(3)[b]	0.50048(2)	0.49913(8)	0.18683(5)	2.08(3)
N(1)[b]	0.4342(2)	0.502(1)	0.0744(6)	2.2(3)
N(2)[b]	0.4351(2)	0.305(1)	−0.0170(5)	2.4(3)
C(1)	0.4183(2)	0.4943(9)	−0.0231(6)	5.2(3)
C(2)	0.3828(2)	0.509(1)	−0.0491(6)	3.3(2)
C(3)	0.3615(1)	0.3666(7)	0.0182(3)	2.4(2)
C(4)	0.3521(1)	0.4256(8)	0.1197(4)	2.6(2)
C(5)	0.3322(1)	0.2963(8)	0.1787(3)	2.8(2)
C(6)	0.3218(1)	0.0979(8)	0.1380(4)	2.8(2)
C(7)	0.3306(1)	0.0346(8)	0.0368(5)	2.9(2)
C(8)	0.3499(1)	0.1668(8)	−0.0212(3)	2.6(2)
F(1)	0.36218(7)	0.6169(5)	0.1639(2)	4.0(1)
F(2)	0.32306(7)	0.3629(6)	0.2773(2)	4.5(2)
F(3)	0.30318(8)	−0.0317(5)	0.1956(3)	4.5(1)
F(4)	0.32014(7)	−0.1581(5)	−0.0050(3)	4.2(1)
F(5)	0.35780(7)	0.0982(6)	−0.1202(2)	4.2(1)
C(9)	0.2349(2)	0.080(2)	0.044(1)	6.7(5)
C(10)	0.2545(2)	0.432(2)	0.060(1)	7.4(5)
C(11)	0.2400(2)	0.261(2)	0.1020(6)	6.9(5)

[a] Hydrogen atom positions and anisotropic thermal parameters are provided as Supporting Information. [b] Occupancy 1/2.

Thermal Analysis. Thermogravimetric analysis (TGA) was conducted with freshly prepared samples on a TA Instruments TGA-2950 under a nitrogen purge of 70 mL/min. Unless otherwise noted, samples were allowed to isothermally purge under nitrogen at ambient temperature (22−25 °C) for 20 min prior to being heated at a constant rate of 5 °C/min from ambient to 600 °C. The deintercalated species was identified by employing tandem TGA−FTIR using a Nicolet TGA interface and a Nicolet Magna 760 spectrometer. The glass-lined transfer line and the gas-phase cell of the interface were maintained at 200 °C to prevent condensation of volatiles. The nitrogen purge of the TGA instrument at 70 mL/min was used as carrier gas. Time-resolved collection of spectra and generation of Gram−Schmidt plots (integrated total IR signal as a function of time) allowed correlation with the TGA thermograms. For each spectrum collected, 64 scans at 4 cm^{-1} resolution

(42) Sheldrick, G. M. SADABS, Institut für Anorganische Chemie der Universität Göttingen, Göttingen, Germany, 1997.
(43) Gabe, E. J.; Le Page, Y.; Charland, J.-P.; Lee, F. L.; White, P. S. *J. Appl. Crystallogr.* **1989**, *22*, 384.
(44) Le Page, Y. *J. Appl. Crystallogr.* **1988**, *21*, 983.

Table 3. Positional and Thermal Parameters[a] for $(C_6H_5C_2H_4NH_3)_2SnI_4\cdot(C_6F_6)$

atom	x	y	z	B_{iso} (Å^2)
Sn	0.50	0.01007(7)	0.25	2.41(2)
I(1)	0.421282(8)	0.01068(5)	0.23037(3)	2.09(1)
I(2)[b]	0.49971(2)	0.1214(1)	0.00061(5)	1.77(2)
I(3)[b]	0.50008(2)	0.50831(9)	0.18980(6)	1.84(3)
N(1)[b]	0.4344(2)	0.512(1)	0.0687(7)	2.0(3)
N(2)[b]	0.4349(2)	0.688(1)	−0.0098(7)	1.9(3)
C(1)	0.4202(2)	0.482(1)	−0.0311(8)	4.7(4)
C(2)	0.3847(2)	0.458(1)	−0.0545(6)	3.4(3)
C(3)	0.3631(1)	0.6113(9)	0.0076(4)	2.2(2)
C(4)	0.3529(2)	0.562(1)	0.1127(5)	2.8(2)
C(5)	0.3346(2)	0.707(1)	0.1686(5)	3.8(3)
C(6)	0.3251(2)	0.905(1)	0.1225(6)	4.2(3)
C(7)	0.3341(2)	0.956(1)	0.0197(6)	3.6(3)
C(8)	0.3532(1)	0.814(1)	−0.0368(5)	2.9(2)
C(9)	0.2313(1)	0.886(1)	0.0594(5)	2.9(2)
C(10)	0.2601(2)	0.5504(9)	0.0420(5)	3.0(2)
C(11)	0.2413(2)	0.685(1)	0.1023(5)	3.3(3)
F(1)	0.2122(1)	1.0176(7)	0.1186(4)	5.9(2)
F(2)	0.2706(1)	0.3578(6)	0.0837(3)	5.3(2)
F(3)	0.2322(1)	0.6213(9)	0.2017(3)	6.1(2)

[a] Hydrogen atom positions and anisotropic thermal parameters are provided as Supporting Information. [b] Occupancy 1/2.

Table 4. Selected Bond Distances (Å) and Angles (deg) for $(C_6F_5C_2H_4NH_3)_2SnI_4\cdot(C_6H_6)$

SnI−(1)	3.1653(9)	I(1)−Sn−I(3)[a]	89.30(1)
SnI−(1)[a]	3.1653(9)	I(1)−Sn−I(3)[d]	90.70(1)
SnI−(2)	3.0944(9)	I(1)[a]−Sn−I(2)	90.32(1)
SnI−(2)[c]	3.227(1)	I(1)[a]−Sn−I(2)[c]	88.68(1)
SnI−(3)[a]	3.101(1)	I(1)[a]−Sn−I(3)[a]	89.52(1)
SnI−(3)[d]	3.226(1)	I(1)[a]−Sn−I(3)[d]	90.49(1)
		I(2)−Sn−I(2)[c]	178.11(2)
Sn−I(2)−Sn[b]	151.23(3)	I(2)−Sn−I(3)[a]	90.89(2)
Sn[e]−I(3)−Sn	151.62(2)	I(2)−Sn−I(3)[d]	89.68(2)
I(1)−Sn−I(1)[a]	178.77(2)	I(2)[c]−Sn−I(3)[a]	90.70(2)
I(1)−Sn−I(2)	89.39(1)	I(2)[c]−Sn−I(3)[d]	88.73(2)
I(1)−Sn−I(2)[c]	91.64(1)	I(3)[a]−Sn−I(3)[d]	179.43(2)

[a] $1-x, y, 0.5-z$. [b] $1-x, -y, -z$. [c] $x, -y, 0.5+z$. [d] $x, -1+y, z$. [e] $x, 1+y, z$.

Table 5. Selected Bond Distances (Å) and Angles (deg) for $(C_6H_5C_2H_4NH_3)_2SnI_4\cdot(C_6F_6)$

Sn−I(1)	3.1985(5)	I(1)−Sn−I(3)[a]	90.14(2)
Sn−I(1)[a]	3.1985(5)	I(1)−Sn−I(3)[d]	89.86(2)
Sn−I(2)	3.1074(7)	I(1)[a]−Sn−I(2)	91.32(1)
Sn−I(2)[c]	3.1519(7)	I(1)[a]−Sn−I(2)[c]	89.13(1)
Sn−I(3)[a]	3.1167(8)	I(1)[a]−Sn−I(3)[a]	89.73(2)
Sn−I(3)[d]	3.1376(8)	I(1)[a]−Sn−I(3)[d]	90.27(2)
		I(2)−Sn−I(2)[c]	177.84(2)
Sn−I(2)−Sn[b]	152.73(3)	I(2)−Sn−I(3)[a]	91.01(2)
Sn[e]−I(3)−Sn	152.91(2)	I(2)−Sn−I(3)[d]	89.08(2)
I(1)−Sn−I(1)[a]	179.87(2)	I(2)[c]−Sn−I(3)[a]	91.10(2)
I(1)−Sn−I(2)	88.65(1)	I(2)[c]−Sn−I(3)[d]	88.81(2)
I(1)−Sn−I(2)[c]	90.90(1)	I(3)[a]−Sn−I(3)[d]	179.90(2)

[a] $1-x, y, 0.5-z$. [b] $1-x, -y, -z$. [c] $x, -y, 0.5+z$. [d] $x, -1+y, z$. [e] $x, 1+y, z$.

were averaged. Neat samples of benzene and hexafluorobenzene were also introduced to the FTIR gas cell by being heated in the TGA instrument, allowing confirmation of the deintercalate identity.

Differential scanning calorimetry (DSC) thermograms were collected on a TA Instruments MDSC-2920 under a nitrogen purge of 70 mL/min. Unless otherwise noted, the heating rate used was 5 °C/min. The DSC temperature scale was calibrated at the 5 °C/min ramp rate using the indium melting transition (measured, 156.8 °C; expected, 156.6 °C). Freshly prepared samples were weighed into Al pans and sealed. A small hole was made in each sample pan to allow evolution of developed gases. Samples were referenced to an empty pan with a lid. Transition temperatures reported are the onset of each thermal event, unless noted otherwise.

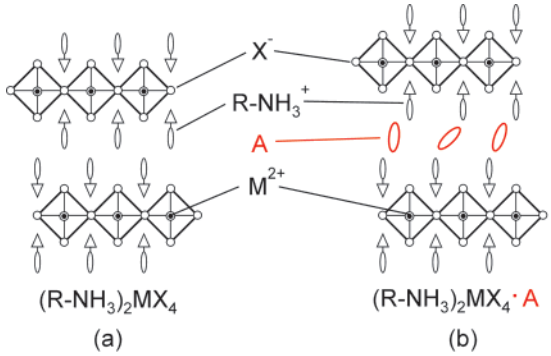

Figure 1. Schematic representation of (a) unintercalated and (b) intercalated $(R-NH_3)_2MX_4$ layered perovskites. In the current study, the MX_4^{2-} framework is SnI_4^{2-}, the organic cation is either phenethylammonium or 2,3,4,5,6-pentafluorophenethylammonium, and the intercalated molecule, A, is either hexafluorobenzene or benzene.

Optical Properties. Absorption spectra were obtained at room temperature on spin-coated films (deposited on quartz disks) of each unintercalated and corresponding intercalated hybrid, using a Hewlett-Packard UV−vis 8543 spectrophotometer.

Results and Discussion

Intercalation and the Fluoroaryl−Aryl Interaction. The basic building block of the hybrid perovskite structure consists of well-ordered anionic layers of corner-sharing metal halide octahedra (MX_4^{2-}), with a layer of organic ammonium cations ($R-NH_3^+$) capping each inorganic sheet on both sides (Figure 1a). The organic cations are hydrogen bonded to halogens in the inorganic sheet through the pendant ammonium group. The full three-dimensional structure is created by stacking the neutral organic-sheathed perovskite layers along the *a* axis. Weak (e.g., van der Waals) interactions between the organic tail groups of successive perovskite layers hold the structure together, with essentially no interleaving among aromatic and short aliphatic organic cations from adjacent layers. The van der Waals gap between organic cations appears to be ideally suited for the intercalation of suitably designed molecular species (Figure 1b), which have the potential for a wide range of interactions with the organic cation layer, including van der Waals, charge-transfer, and aromatic−aromatic interactions. Note that the organic intercalated species can, in principle, be either ordered or disordered and can fully or partially occupy sites within the intercalating layer.

Fluoroaryl−aryl interaction is one important subclass of noncovalent interaction and is responsible for the anomalously high melting temperatures of equimolar donor−acceptor complexes, such as benzene/hexafluorobenzene (23.7 °C),[35] 2-methylnaphthalene/hexafluorobenzene (56 °C),[35] *p*-xylene/hexafluorobenzene (27.4 °C),[45] mesitylene/hexafluorobenzene (34 °C),[35] and hexamethylbenzene/hexafluorobenzene (∼131 °C).[46] While the fluoroaryl−aryl interaction was originally attributed to $\pi-\pi$ charge transfer,[35]

(45) Dahl, T. *Acta Chem. Scand., A* **1975**, *29*, 170.
(46) Dahl, T. *Acta Chem. Scand.* **1972**, *26*, 1569.

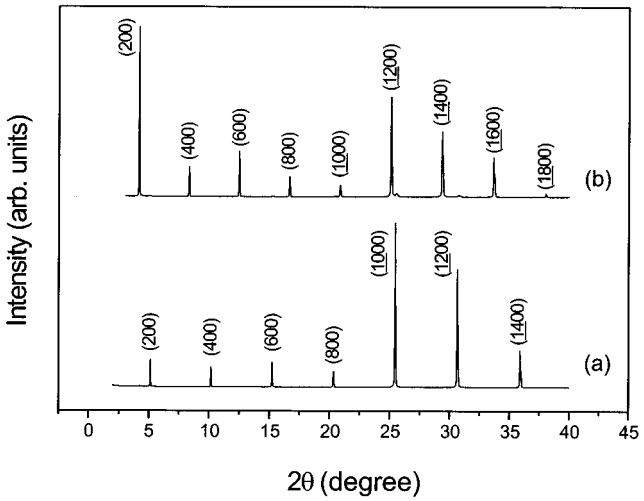

Figure 2. Room-temperature powder X-ray scans for (a) unintercalated $(C_6F_5C_2H_4NH_3)_2SnI_4$ and (b) toluene-intercalated $(C_6F_5C_2H_4NH_3)_2SnI_4$. Note that, for each sample, the crystalline deposit on the slide has a highly preferred (*a* axis) orientation. For the unintercalated material, the refined *d* spacing corresponding to the (2*h*, 0, 0) series of reflections is 35.0(1) Å, whereas for the toluene-intercalated system the corresponding *d* spacing is 42.6(1) Å.

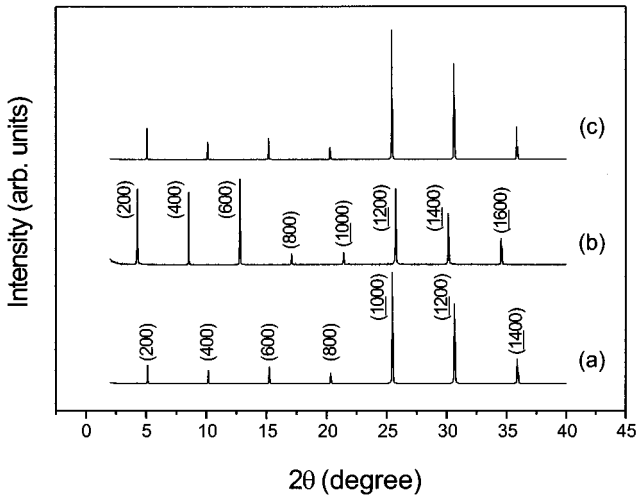

Figure 3. Room-temperature powder X-ray scans for (a) unintercalated $(C_6F_5C_2H_4NH_3)_2SnI_4$ crystals, (b) $(C_6F_5C_2H_4NH_3)_2SnI_4$ crystals grown from a methanol/benzene mixture, and (c) $(C_6F_5C_2H_4NH_3)_2SnI_4$ crystals grown from a methanol/hexafluorobenzene mixture. Note that, for each sample, the crystalline deposit on the slide has a highly preferred (*a* axis) orientation. For (a) and (c), the refined *d* spacings corresponding to the (2*h*, 0, 0) series of reflections are both 35.0(1) Å, whereas for (b) the refined *d* spacing is 41.5(1) Å.

the absence of expected ^{19}F NMR chemical shifts,[36,47] vibrational mode shifts,[48] and "charge-transfer" ultraviolet absorption bands[35,49] failed to support such an interpretation, even for systems involving the powerful hexamethylbenzene donor and hexafluorobenzene. Rather, the stabilization in these systems is more likely electrostatic in origin, with weak hydrogen bonding and van der Waals interactions also playing a role.[36,49] In $C_6H_6{\cdot}C_6F_6$, the large magnitude and opposite polarity of the quadrupole moments for benzene and hexafluorobenzene provide a significant stabilizing influence.[36] The basic ordering of the two species in $C_6H_6{\cdot}C_6F_6$ is an alternating face-to-face stack, whereas for each component alone, the crystal structures adopt a herringbone (T-shaped) packing.[50,51]

The first indication of intercalation in a perovskite system with potential for fluoroaryl−aryl interaction occurred upon trying to recrystallize the 2,3,4,5,6-pentafluorophenethylammonium-based $(C_6F_5C_2H_4NH_3)_2SnI_4$ using a mixed methanol/toluene solvent. Rather than the 35.0(1) Å (2*h*, 0, 0) series of *d* spacings expected for the perovskite compound, a much larger 42.6(1) Å spacing was observed (Figure 2). Upon examination of single-crystal diffraction data for the resulting crystals,[52] the refined structure looked almost identical to the smaller lattice constant material, except that there was a significantly larger space between organic cations in adjacent layers. Subsequent analysis of the X-ray data led to the refinement of a disordered toluene molecule between the fluorinated rings of the organic cations.

In an effort to systematically study the use of fluoroaryl−aryl interactions in intercalated perovskite structures, a series of four intercalation attempts were considered on the basis of the two parent perovskites phenethylammonium tin(II) iodide, $(C_6H_5C_2H_4NH_3)_2SnI_4$, and the corresponding 2,3,4,5,6-pentafluorophenethylammonium analogue, $(C_6F_5C_2H_4NH_3)_2SnI_4$. Attempts were made to intercalate each of these two systems with the simplest unfluorinated and fluorinated aryl moieties—i.e., benzene and hexafluorobenzene. Note that these molecules are donor−acceptor molecules and also have large quadrupole moments with opposite polarity (-2.9×10^{-39} versus 3.2×10^{-39} C m^2, respectively).[36] The prospective intercalated crystals were grown using a similar process for each system. The parent perovskite materials were first dissolved in a methanol solution containing a large excess of the targeted intercalating species. The solutions were then allowed to partially evaporate at room temperature, until a substantial yield of the red crystals formed. After filtering, the crystals were dried in a vacuum at room temperature for 10−15 min.

Figures 3 and 4 show powder diffraction data from the crystals that resulted from the crystallization of 2,3,4,5,6-pentafluorophenethylammonium-based and phenethylammonium-based perovskites, respectively. For the $(C_6F_5C_2H_4NH_3)_2SnI_4$ parent structure, the unintercalated material (grown by evaporating a methanol or ethanol solution of the perovskite with no intercalating species) exhibited a progression of (2*h*, 0, 0) reflections corresponding to a *d* spacing of 35.0(1) Å (Figure 3a). Growth of crystals from a methanol/benzene solution yielded the diffraction pattern in Figure 3b, with a corresponding *d* spacing of 41.5(1) Å. As described later in the Crystal Structures section, this phase corresponds to a benzene-intercalated $(C_6F_5C_2H_4NH_3)_2SnI_4$ structure [the

(47) Foster, R.; Fyfe, C. A. *J. Chem. Soc., Chem. Commun.* **1965**, 642.
(48) (a) Laposa, J. D.; McGlinchey, M. J., Montgomery, C. *Spectrochim. Acta* **1983**, *39A*, 863. (b) Williams, J. H. *Chem. Phys.* **1992**, 215.
(49) Filler, R. In *Fluorine-containing molecules: structure, reactivity, synthesis, and applications*; Liebman, J. F., Greenberg, A., Dolbier, W. R., Jr., Eds.; VCH Publishers: New York, 1988; pp 19−41.
(50) Boden, N.; Davis, P. P.; Stam, C. H.; Wesselink, G. A. *Mol. Phys.* **1973**, *25*, 81.
(51) Cox, E. G.; Cruickshank, D. W. J.; Smith, J. A. S. *Proc. R. Soc. London, A* **1958**, *247*, 1.
(52) Mitzi, D. B.; Malenfant, P. R. L. Unpublished work.

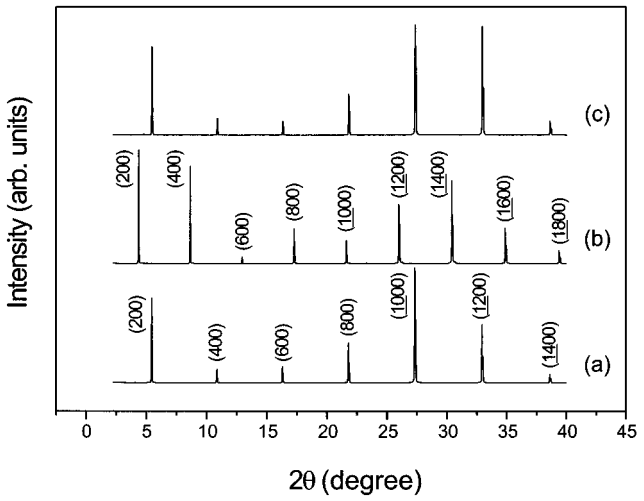

Figure 4. Room-temperature powder X-ray scans for (a) unintercalated $(C_6H_5C_2H_4NH_3)_2SnI_4$ crystals, (b) $(C_6H_5C_2H_4NH_3)_2SnI_4$ crystals grown from a methanol/hexafluorobenzene mixture, and (c) $(C_6H_5C_2H_4NH_3)_2SnI_4$ crystals grown from a methanol/benzene mixture. Note that, for each sample, the crystalline deposit on the slide has a highly preferred (*a* axis) orientation. For (a) and (c), the refined *d* spacings corresponding to the (2*h*, 0, 0) series of reflections are both 32.6(1) Å, whereas for (b) the refined *d* spacing is 41.2(1) Å.

single-crystal structure was solved at −75 °C and therefore yields a slightly smaller *d* spacing, $a \sin \beta = 40.99(1)$ Å]. Note that this powder diffraction pattern is quite stable with respect to time. Repeating the diffraction pattern eight times over a period of 24 h indicated essentially no change in the profile. Growth of crystals from a methanol/hexafluorobenzene solution yielded crystals with a progression of (2*h*, 0, 0) reflections corresponding to a *d* spacing of 35.0(1) Å (Figure 3c), identical to the parent material and indicating essentially no stable intercalation taking place. A similar situation resulted for the analogous phenethylammonium-based perovskite systems, with, however, the hexafluorobenzene cosolvent resulting in the intercalated structure and the benzene crystallization run leading to essentially no intercalated materials (Figure 4). It should be noted that for experiments using organic cations and intercalating species that are either both fluorinated or unfluorinated, when the crystals are put on the slide wet and immediately placed in the X-ray diffraction apparatus, small amounts of a larger axis species can sometimes be observed. However, when the crystals are gently dried (in the same way as the other systems studied—i.e., by placing the crystals in a vacuum at room temperature for 10−15 min), this minor phase disappears, leaving behind the unintercalated parent compound. The four intercalation experiments therefore clearly demonstrate that, in the current systems, the most stable intercalated structures are formed when the organic cation and the intercalating species have the possibility of a fluoroaryl−aryl interaction—i.e., either when the organic cation phenyl ring is fluorinated and the intercalated molecule has an unfluorinated ring or vice versa.

Crystal Structures. The monoclinic (*C*2/*c*) subcells for the two intercalated systems reported in this paper (Figure 5) are analogous to that previously reported for (2-FPEA)$_2$SnI$_4$ and (3-FPEA)$_2$SnI$_4$ (with, however, the inclusion

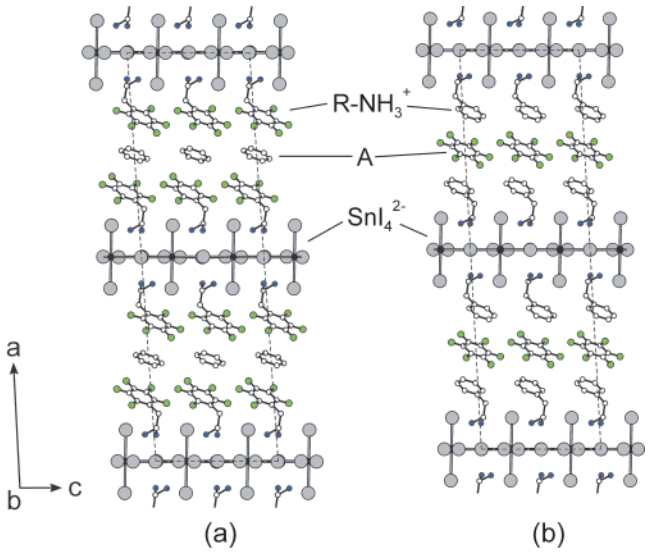

Figure 5. Crystal structures of (a) $(C_6F_5C_2H_4NH_3)_2SnI_4 \cdot (C_6H_6)$ and (b) $(C_6H_5C_2H_4NH_3)_2SnI_4 \cdot (C_6F_6)$, viewed down the *b* axis. Dashed lines depict the unit cell outlines. For clarity, the atoms are represented as spheres with uniform sizes selected for each atom type and fluorine atoms are colored green.

of an intercalated layer),[21] where *n*-FPEA corresponds to *n*-fluorophenethylammonium and $n = 2$ or 3 denotes the position of fluorine substitution. In the low-temperature cell for $(C_6F_5C_2H_4NH_3)_2SnI_4 \cdot (C_6H_6)$, the inorganic sheets are derived from one crystallographically independent distorted SnI_6 octahedron, with bridging Sn−I bond lengths (Table 4) ranging from 3.0944(9) to 3.227(1) Å (the bridging iodides are disordered with equal probability between two symmetry-related sites) and two terminal Sn−I(1) bonds of length 3.1653(9) Å. The average Sn−I bond length is 3.163 Å. The analogous data for $(C_6H_5C_2H_4NH_3)_2SnI_4 \cdot (C_6F_6)$ indicate that the octahedra are less distorted (Table 5), with bridging bond lengths ranging from 3.1074(7) to 3.1519(7) Å and terminal bonds of length 3.1985(5) Å. The average Sn−I bond length, 3.152 Å, is shorter than that for the pentafluorophenethylammonium tin(II) iodide analogue, consistent with the darker coloration for the phenethylammonium compound.[7] The inorganic framework and organic cations in each intercalated structure adopt a configuration virtually identical to that found in the unintercalated parent compounds,[53] with the organic cations in a J-shaped (or gauche) conformation[21,54] and a herringbone packing of the phenyl or pentafluorophenyl moieties within a given cation layer. The prevalence of the herringbone packing arrangement can be understood in terms of edge-to-face (tilted-T) aromatic interactions among the aromatic moieties.[2,55−58]

The intercalated molecule in each hybrid structure is sandwiched between two aryl groups from organic cations

(53) (a) Papavassiliou, G. C.; Koutselas, I. B.; Terzis, A.; Whangbo, M.-H. *Solid State Commun.* **1994**, *91*, 695. (b) Mitzi, D. B.; Malenfant, P. R. L. Unpublished work.
(54) Mitzi, D. B. *J. Solid State Chem.* **1999**, *145*, 694.
(55) Barclay, T. M.; Cordes, A. W.; MacKinnon, C. D.; Oakley, R. T.; Reed, R. W. *Chem. Mater.* **1997**, *9*, 981.
(56) Hunter, C. A.; Sanders, J. K. M. *J. Am. Chem. Soc.* **1990**, *112*, 5525.
(57) Paliwal, S.; Geib, S.; Wilcox, C. S. *J. Am. Chem. Soc.* **1994**, *116*, 4497.
(58) Jorgensen, W. L.; Severance, D. L. *J. Am. Chem. Soc.* **1990**, *112*, 4768.

in adjacent layers (Figure 5). The phenyl component of the organic cation and the intercalated molecule exhibit only slight deviations from planarity. For $(C_6F_5C_2H_4NH_3)_2SnI_4\cdot(C_6H_6)$, the pentafluorophenyl carbon atoms are all within 0.010(5) Å of the least-squares best plane for the ring, whereas the fluorines are slightly displaced from this plane [e.g., the largest deviations are −0.035(4) Å for F(2) and 0.026(4) Å for F(3)]. For the intercalated benzene molecule, the carbons are all within 0.01(2) Å of the least-squares best plane. There is a small dihedral angle [7.8(8)°] between the best planes formed by the cation and benzene rings. The center-to-center distance between the 2,3,4,5,6-pentafluorophenyl moiety and the intercalated benzene is 3.810 Å (symmetric on each side of the benzene molecule). Within the pentafluorophenyl/benzene/pentafluorophenyl sandwich, close interactions between the organic cation and the benzene molecule include C(7)···C(11)* [3.490(8) Å] (where the asterisk indicates an atom from the benzene molecule), C(6)···C(11)* [3.504(8) Å], F(3)···C(11)* [3.296(8) Å], and F(3)···C(9)* [3.326(8) Å]. These distances are consistent with (but, for the C···C bonds, slightly smaller than) the sum of van der Waals radii for aromatic carbon (1.77 Å) and fluorine (1.47 Å) atoms.[59] There are also significant interactions between each intercalated benzene and nearest-neighbor pentafluorophenethylammonium cations and benzene molecules (i.e., those in neighboring pentafluorophenyl/benzene/pentafluorophenyl stacks), which may help to stabilize the observed configuration. These interstack interactions, which are similar in length to the interatomic contacts between adjacent columns of benzene and hexafluorobenzene molecules in the low-temperature phase of $C_6H_6\cdot C_6F_6$,[60] include F(3)···C(11)* [3.395(8) Å], F(3)···H(C11)* [2.57(8) Å], and H(C9)*···H(C10)* [2.6(1) Å]. Short C−F···H−C intermolecular interactions (i.e., with F···H distances of 2.4−2.7 Å) have been observed in a number of other fluoroaryl−aryl systems and may indicate hydrogen bonding interactions, although favorable packing or lateral quadrupolar interactions may also account for the short distances.[38−40,61]

For $(C_6H_5C_2H_4NH_3)_2SnI_4\cdot(C_6F_6)$, the phenyl carbons and hexafluorobenzene molecule are also essentially coplanar (the phenyl hydrogens are also coplanar to within the relatively large positional uncertainty for these atoms). The dihedral angle between the best planes for the phenyl and hexafluorobenzene moieties is 1.4(3)°, smaller than that for $(C_6F_5C_2H_4NH_3)_2SnI_4\cdot(C_6H_6)$. The center-to-center distance between the phenyl component and the hexafluorobenzene molecule is 3.858 Å. Within the phenyl/hexafluorobenzene/phenyl sandwich, close interactions between the organic cation and the hexafluorobenzene molecule include C(7)···C(11)* [3.44(1) Å] (where the asterisk indicates the hexafluorobenzene molecule), C(5)···C(10)* [3.457(9) Å], and C(7)···C(9)* [3.470(9) Å]. These distances are all significantly smaller than the sum of van der Waals radii for two aromatic carbons (3.54 Å).[59] Besides the interactions within a phenyl/hexafluorobenzene/phenyl sandwich, there are also significant interactions between each intercalated hexafluorobenzene molecule and phenethylammonium cations and hexafluorobenzene molecules in adjacent sandwich structures, including F(2)*···F(2)* [2.878(8) Å], F(3)*···H(C6) [2.70(8) Å], and F(1)*···H(C5) [2.76(7) Å].

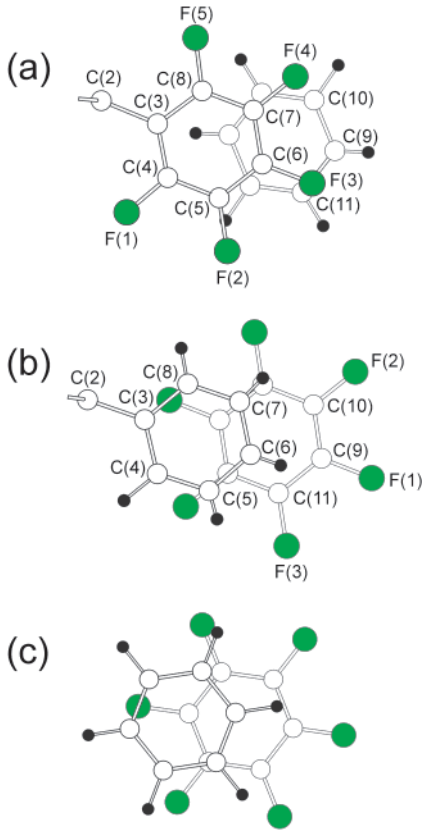

Figure 6. Face-to-face aromatic interaction in (a) $(C_6F_5C_2H_4NH_3)_2SnI_4\cdot(C_6H_6)$, (b) $(C_6H_5C_2H_4NH_3)_2SnI_4\cdot(C_6F_6)$, and (c) $C_6H_6\cdot C_6F_6$. The view is nominally perpendicular to the plane of the phenyl rings. For the two new compounds (a, b), atom labeling for the carbon and fluorine atoms is indicated in the figure. For clarity, in (a) and (b), only one organic cation is shown interacting with the intercalated molecule.

Each intercalated molecule in the perovskite structures occupies a position sandwiched between two aromatic cations (Figure 5), with an offset face-to-face interaction between the two cations and the aromatic intercalated molecule (Figure 6a,b). Note that the $C_6H_6\cdot C_6F_6$ complex consists of columns of alternating benzene and hexafluorobenzene molecules, with a similar type of interaction between the aromatic moieties (Figure 6c).[60] As for the current structures, close intermolecular C···C contacts (3.36−3.54 Å) between neighboring benzene and hexafluorobenzene molecules within each column are shorter than twice the aromatic carbon van der Waals radius and are indicative of a favorable face-to-face interaction. In contrast, for crystals of benzene or hexafluorobenzene, which adopt an edge-to-face packing, no C···C contacts shorter than 3.6 Å appear in the structures.[50,51]

In the current structures, the tethering of the organic cations to the inorganic framework has two important implications. First, the extended framework of tin(II) iodide octahedra and

(59) Bondi, A. *J. Phys. Chem.* **1964**, *68*, 441.
(60) Williams, J. H.; Cockcroft, J. K.; Fitch, A. N. *Angew. Chem., Int. Ed. Engl.* **1992**, *31*, 1655.
(61) Ponzini, F.; Zagha, R.; Hardcastle, K.; Siegel, J. S. *Angew. Chem., Int. Ed.* **2000**, *39*, 2323.

ionically bonded (also with hydrogen bonding) organic cations provides a robust matrix into which the intercalating molecules can be incorporated, thereby leading to substantial thermal stability (in contrast to $C_6H_6 \cdot C_6F_6$, the hybrid solids are stable well above room temperature). In addition, the herringbone arrangement of the organic cation phenyl rings imposes a specific ordering to the corresponding intercalated molecules. Note that the inorganic framework can be used to control the ordering of the aromatic cations. For example, in $(C_6H_5C_2H_4NH_3)_2CuCl_4$, the organic cations are held in a distinct orientation and conformation compared with those in the corresponding tin(II) iodide-based system, as a result of the Jahn−Teller distortion of the $CuCl_6$ octahedra.[54,62] The phenyl ring orientation in $(C_6H_5C_2H_4NH_3)_2CuCl_4$ is such that the plane of each ring is nearly perpendicular to the inorganic sheets (a ∼80° angle between the two planes) and is mutually perpendicular to its nearest neighbors within a given layer.[62] This orientation is not conducive for the formation of the cation 1/hexafluorobenzene/cation 2 stacking of the intercalated systems stabilized by fluoroaryl−aryl interaction, where cation 1 and cation 2 are on adjacent organic cation layers. In $(C_6H_5C_2H_4NH_3)_2SnI_4$, the phenyl rings lie more flat with respect to the inorganic sheets (a ∼32 ° angle between the planes),[53] thereby enabling more facile aromatic−aromatic stacking between layers. Preliminary attempts to intercalate hexafluorobenzene in the copper(II) chloride system, using a crystal growth process similar to that used for the tin(II) iodides, were unsuccessful (i.e., only unintercalated materials were achieved), presumably as a result of the unfavorable organic cation packing in this system. An interesting area of further study involves examining how other hybrid perovskite frameworks, along with fluoroaryl−aryl interaction, can be used to control the relative ordering and contact between neighboring intercalated molecules within the hybrid structures.

Thermal Analysis. TGA of $(C_6F_5C_2H_4NH_3)_2SnI_4 \cdot (C_6H_6)$ and $(C_6H_5C_2H_4NH_3)_2SnI_4 \cdot (C_6F_6)$ crystals yields a weight loss transition, below the decomposition point of the parent perovskite, which corresponds to the complete loss of the intercalated species. For $(C_6F_5C_2H_4NH_3)_2SnI_4 \cdot (C_6H_6)$ crystals, the deintercalation process has an onset at 145(2) °C and a corresponding mass loss of 7.1(5)% (Figure 7), consistent with the predicted value of 6.9% for the complete loss of benzene from the perovskite. The measured weight loss is therefore consistent with full occupancy of the benzene site in the original intercalated structure, in agreement with the structural and chemical analysis data. The Gram−Schmidt plot of the evolved gas (Figure 8) shows a substantial peak at the same time as the weight loss transition in the TGA data, with an FTIR spectrum for the corresponding evolved species identical to that obtained for pure benzene (Figure 8, inset). In the TGA data for $(C_6F_5C_2H_4NH_3)_2SnI_4$ (Figure 7), the weight loss process centered at ∼250 °C corresponds approximately to the complete loss of pentafluorophenethylammonium iodide from the sample, leaving behind SnI_2 (the calculated weight loss for this process is 64.5%). DSC scans

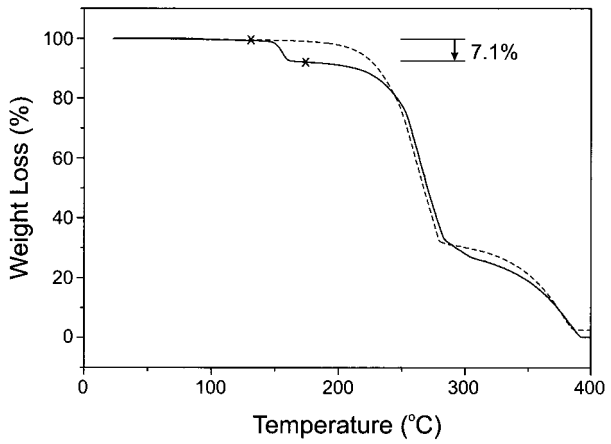

Figure 7. TGA scans for $(C_6F_5C_2H_4NH_3)_2SnI_4$ (dashed line) and $(C_6F_5C_2H_4NH_3)_2SnI_4 \cdot (C_6H_6)$ (solid line) crystals, run at 5 °C/min in a flowing nitrogen atmosphere. The x's on the solid curve indicate the approximate points along the curve for which the calculated weight loss was determined.

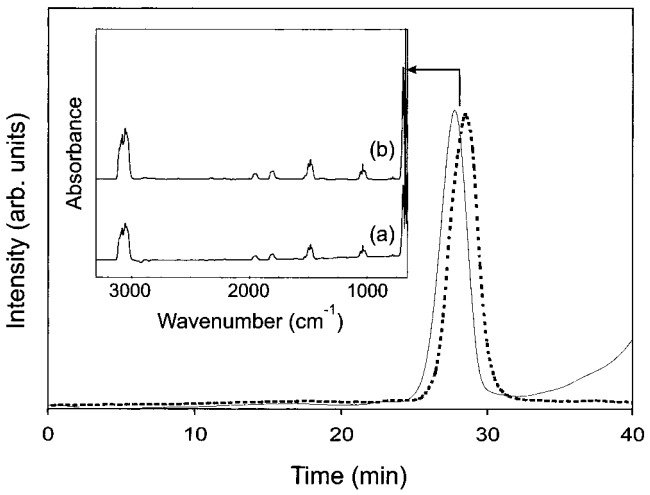

Figure 8. First derivative of the $(C_6F_5C_2H_4NH_3)_2SnI_4 \cdot (C_6H_6)$ TGA scan shown in Figure 7 (solid line) and the corresponding Gram−Schmidt plot of the evolved gas during this scan measured from FTIR analysis (dashed line). The small time shift between the two peaks corresponds to the length of time it takes the evolved gas to diffuse through the capillary to the FTIR apparatus. The inset shows (a) the FTIR spectrum of the evolved gas taken at the peak of the Gram−Schmidt plot and (b) the corresponding FTIR spectrum for pure benzene placed in the TGA−FTIR apparatus.

for both the parent $(C_6F_5C_2H_4NH_3)_2SnI_4$ perovskite and the corresponding benzene-intercalated system are shown in Figure 9a,b, respectively. The parent perovskite exhibits two endothermic transitions at 224(2) and 251(2) °C. The lower temperature transition [20.8(5) kJ/mol] is reversible and most likely corresponds to a structural/premelting transition involving conformational flexibility or changes in the hydrogen-bonding configuration of the phenethylammonium cation.[63] The second transition, which is not completely reversible, corresponds to melting/decomposition, before the material undergoes bulk decomposition at temperatures above ∼260 °C. Note that a similar melting/decomposition transition has been noted for $(C_4H_9NH_3)_2SnI_4$ at 256(2) °C.[11] For the intercalated system, the two endotherms remain unaltered. However, there is also an additional endotherm [12.6(5) kJ/

(62) Willett, R. D. *Acta Crystallogr., C* **1990**, *46*, 565.

(63) Ueda, T.; Omo, M.; Shimizu, K.; Ohki, H.; Okuda, T. *Z. Naturforsch.* **1997**, *52a*, 502.

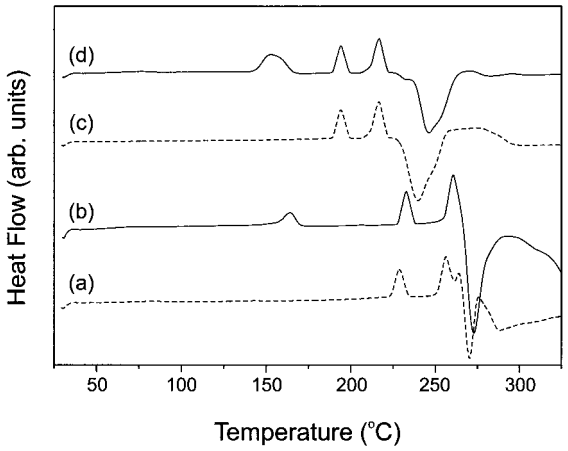

Figure 9. DSC scans for (a) $(C_6F_5C_2H_4NH_3)_2SnI_4$ (dashed line), (b) $(C_6F_5C_2H_4NH_3)_2SnI_4{\cdot}(C_6H_6)$ (solid line), (c) $(C_6H_5C_2H_4NH_3)_2SnI_4$ (dashed line), and (d) $(C_6H_5C_2H_4NH_3)_2SnI_4{\cdot}(C_6F_6)$ (solid line) crystals, run at 5 °C/min in a nonhermetically sealed aluminum capsule. Exothermal peaks are down along the heat flow axis. The important transitions are noted in the text.

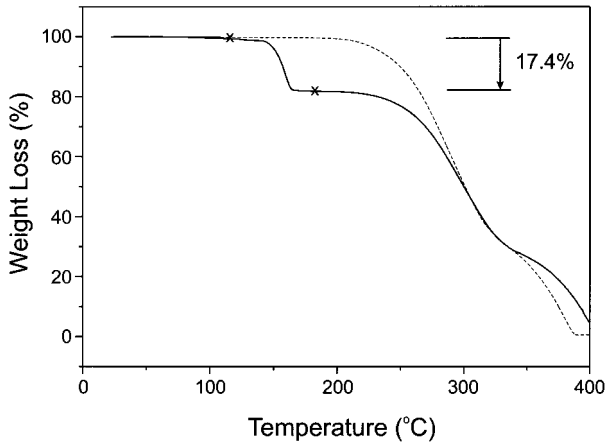

Figure 10. TGA scan of $(C_6H_5C_2H_4NH_3)_2SnI_4$ (dashed line) and $(C_6H_5C_2H_4NH_3)_2SnI_4{\cdot}(C_6F_6)$ (solid line) crystals, run at 5 °C/min in a flowing nitrogen atmosphere. The x's on the solid line indicate the approximate points along this curve for which the calculated weight loss was determined.

mol] at 150(2) °C, corresponding to the deintercalation process. The observed deintercalation temperature is significantly above the boiling temperature of benzene under standard conditions (80 °C).

For $(C_6H_5C_2H_4NH_3)_2SnI_4{\cdot}(C_6F_6)$ crystals, the first weight loss transition also has an onset at 145(2) °C and a corresponding mass loss of 17.4(5)% (Figure 10), consistent with the predicted value of 17.6% for the complete loss of hexafluorobenzene from the perovskite. The Gram−Schmidt plot (Figure 11) shows a substantial peak at the same time as the weight loss transition in the TGA data, with an FTIR spectrum for the species being generated identical to that obtained for pure hexafluorobenzene (Figure 11, inset). The unintercalated $(C_6H_5C_2H_4NH_3)_2SnI_4$ perovskite exhibits two endothermic transitions in the DSC scan at 189(2) °C [20.2(5) kJ/mol] and 210(2) °C [30.2(5) kJ/mol] (Figure 9c). These transitions likely have an origin similar to those of the corresponding two transitions in $(C_6F_5C_2H_4NH_3)_2SnI_4$, although shifted to lower temperature. Visual examination of the crystals in a sealed tube as a function of temperature

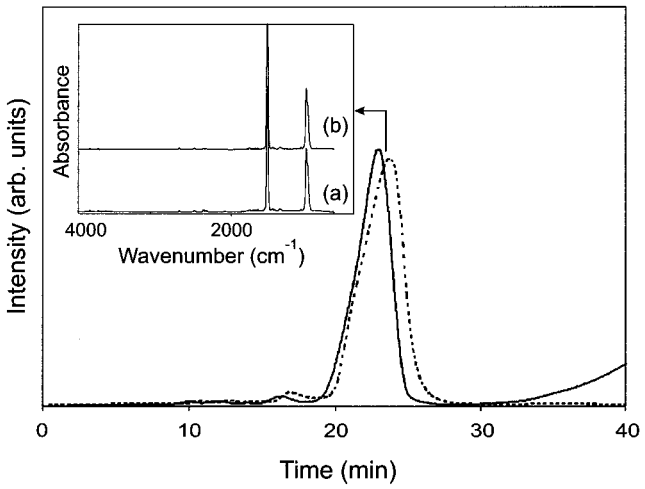

Figure 11. First derivative of the TGA scan for $(C_6H_5C_2H_4NH_3)_2SnI_4{\cdot}(C_6F_6)$ shown in Figure 10 (solid line) and the corresponding Gram−Schmidt plot of the evolved gas during this scan measured from FTIR analysis (dashed line). The inset shows (a) the FTIR spectrum of the evolved gas taken at the peak of the Gram−Schmidt plot and (b) the corresponding FTIR spectrum for pure hexafluorobenzene placed in the TGA−FTIR apparatus.

confirms that the 210(2) °C process involves a melting transition. For the intercalated system (Figure 9d), the two endotherms remain unaltered, with, however, an additional deintercalation endotherm [32.1(8) kJ/mol] at 143(2) °C.

For each intercalated system, the exact temperature and sharpness of the weight loss transition in the TGA trace depend on the grain size of the crystals used for the run. For very-fine-grained precipitated materials, the weight loss transition broadens and shifts to lower temperature. For these finer grained materials, the intercalated molecule has a shorter distance to diffuse to leave the crystals. However, perhaps more importantly, with an increased surface-to-volume ratio, a relatively larger amount of the intercalating species might also be simply surface bound, thereby interacting with only a single organic cation. As a result of this latter factor, only the thermal analysis results of the better crystallized materials are presented here. Note that thermal analysis runs on the $(C_6H_5C_2H_4NH_3)_2SnI_4{\cdot}(C_6F_6)$ crystals were performed at 1 and 10 °C/min, in addition to the standard 5 °C/min scans. In each case, only slight shifts (<2 °C) in the onset temperature of the deintercalation process were noted.

On the basis of the thermal analysis results on the intercalated systems, the $(C_6F_5C_2H_4NH_3)_2SnI_4{\cdot}(C_6H_6)$ and $(C_6H_5C_2H_4NH_3)_2SnI_4{\cdot}(C_6F_6)$ crystals were examined using powder X-ray diffraction before and after anneals of between 25 and 35 min at 175 °C on a temperature-controlled hot plate contained within a drybox (the crystals were confined between two glass plates placed on the hot plate). As seen in Figures 12 and 13, after the appropriate annealing sequence, the parent compounds were recovered from the intercalated crystals. The temperature and duration of the anneal are important since if the crystals are annealed at a lower temperature or for too short a time, the resulting powder pattern reveals a mixed-phase sample containing both the intercalated and unintercalated analogues of the hybrid. If the sample is annealed too long or at a substantially higher

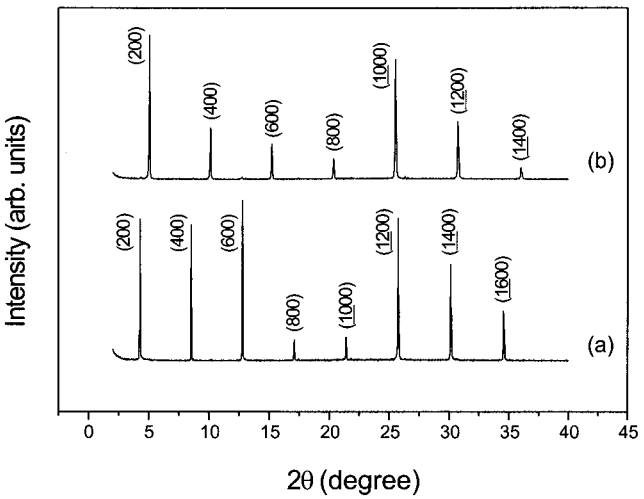

Figure 12. Room-temperature powder X-ray scans for (a) intercalated $(C_6F_5C_2H_4NH_3)_2SnI_4 \cdot C_6H_6$ crystals and (b) intercalated crystals from the same batch that have been annealed at 175 °C for 35 min. For (a) the refined *d* spacing corresponding to the (2*h*, 0, 0) series of reflections is 41.5(1) Å, whereas for (b) the corresponding *d* spacing is 34.9(1) Å.

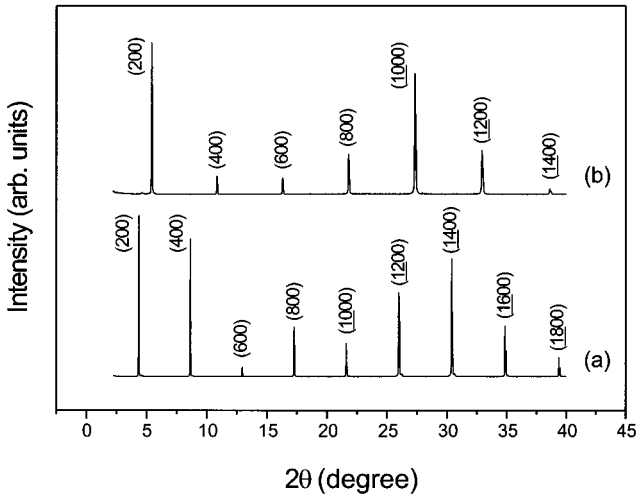

Figure 13. Room-temperature powder X-ray scans for (a) intercalated $(C_6H_5C_2H_4NH_3)_2SnI_4 \cdot C_6F_6$ crystals and (b) intercalated crystals from the same batch that have been annealed at 175 °C for 25 min. For (a) the refined *d* spacing corresponding to the (2*h*, 0, 0) series of reflections is 41.2(1) Å, whereas for (b) the corresponding *d* spacing is 32.6(1) Å.

temperature, extra peaks will appear in the diffraction pattern as a result of the slow thermal decomposition of the material (also evident in the TGA scans of the hybrids).

Optical Properties. Organic−inorganic hybrids of the form $(R-NH_3)_2MI_4$ [M = Ge(II), Sn(II), or Pb(II)] crystallize as self-assembled quantum well structures, typically with smaller band gap inorganic sheets alternating with larger HOMO−LUMO gap organic layers. Sharp resonances in the room-temperature optical absorption spectra of these systems arise from an exciton state associated with the semiconducting inorganic sheets.[9−11,31] In the layered tin(II) iodide materials, for example, the lowest exciton state arises from excitations between the valence band, which consists of a hybridization of Sn(5s) and I(5p) states, and the conduction band, which derives primarily from Sn(5p) states.[53] In addition to tailoring the position of the optical features by making substitutions on the metal or halogen sites, control over the specific structure of the metal halide sheets, and therefore on the electronic structure of this framework, can also be provided by making substitutions on the organic cation site.[21] In the family, $(n\text{-FPEA})_2SnI_4$, for example, where *n*-FPEA = *n*-fluorophenethylammonium and $n = 2$, 3, or 4, the position of the fluorine substitution on the phenyl ring of the cation has an important impact on the electronic and optical properties. Specifically, the exciton state shifts to lower energy, progressing from the 2-FPEA system (588 nm, 2.11 eV) to the 3-FPEA (599 nm, 2.07 eV) and 4-FPEA (609 nm, 2.04 eV) systems, with a corresponding band edge shift for the three systems.[21] The shift in optical properties reflects the progressive shift in structure of the tin(II) iodide framework, including the Sn−I−Sn bond angle (basically a measure of relative rotation among the SnI_6 octahedra within a SnI_4^{2-} sheet) and the average Sn−I bond length, as a function of the fluorine substitution site. Specifically, as the Sn−I−Sn bond angle shifts further from 180° and the average Sn−I bond length increases, the band gap of the semiconducting sheets correspondingly increases.

In each of the $(n\text{-FPEA})_2SnI_4$ systems, the separation between layers remains approximately the same (to within 0.3 Å). The current set of intercalated samples therefore provides an interesting opportunity to probe the effect of increasing the interlayer separation on the electronic and optical properties. Even with unaltered bonding in the inorganic sheets, significant interlayer coupling in the parent compound should lead to a shift in the spectral features to higher energy upon intercalation, as a result of further isolation of the semiconducting layers (i.e., the quantum wells).[64] On the other hand, if the parent materials are already electronically two-dimensional, with very little coupling between the semiconducting inorganic layers, increasing the interlayer separation should have little or no effect on the spectra. Other potential influences of the intercalated species could include electrostatic interactions with the inorganic layers and subtle changes in the bonding of the inorganic framework as described above.

Figure 14 shows the room-temperature absorption spectra for thin films of $(C_6H_5C_2H_4NH_3)_2SnI_4$, as well as for the intercalated analogue $(C_6H_5C_2H_4NH_3)_2SnI_4 \cdot (C_6F_6)$. In $(C_6H_5C_2H_4NH_3)_2SnI_4$, the interlayer separation between the perovskite sheets is 16.3 Å at room temperature, whereas this distance increases to 20.6 Å for the hexafluorobenzene-intercalated system. Despite the 26% increase in interlayer separation, the exciton peak in the absorption spectrum shifts only slightly to higher energy, from 608(2) nm [2.04 eV] for the parent compound to 595(2) nm [2.08 eV] for the intercalated analogue. The band edge peak correspondingly shifts from 520(2) to 510(2) nm. The small magnitude of the spectral shift highlights the two-dimensional nature of the phenethylammonium-based perovskite structures. As for the $C_6H_6 \cdot C_6F_6$ complex,[35] no evidence of a charge-transfer band (between the pentafluorophenyl group and the benzene molecule) can be found at wavelengths above 300 nm (below 300 nm, the absorption from the polycarbonate overlayer

(64) Papavassiliou, G. C. *Prog. Solid State Chem.* **1997**, *25*, 125.

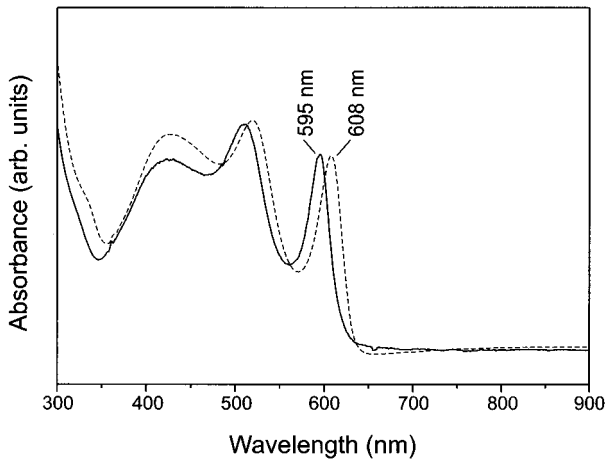

Figure 14. Room-temperature UV−vis absorption spectra for spin-coated thin films of $(C_6H_5C_2H_4NH_3)_2SnI_4$ (dashed line) and $(C_6H_5C_2H_4NH_3)_2SnI_4 \cdot C_6F_6$ (solid line) on quartz disks. In each case, a polycarbonate film has been placed over the sample.

dominates the spectra). For the intercalated films, a low-temperature anneal at 60 °C on a hot plate within a drybox for 30 min leads to complete deintercalation and recovery of the spectrum of the parent compound.

While it is tempting to attribute the small spectral shift to reduced coupling between the semiconducting sheets upon intercalation, perhaps a more reasonable explanation can be derived from the changes in the tin(II) iodide sheet structure induced by the intercalating molecules. A preliminary low-temperature (−75 °C) structural analysis[65] of $(C_6H_5C_2H_4NH_3)_2SnI_4$, for example, leads to a lattice isostructural with that found at room temperature.[53,65] The average Sn−I distances are 3.144 Å for the low-temperature data versus 3.150 Å for the room-temperature data. In addition, the Sn−I−Sn bond angles are 156.55(2)° and 155.56(2)° for the low-temperature data, very similar to the values (156.88° and 156.20°) for the room-temperature data. The intercalated structure has a larger average Sn−I bond length (3.152 Å) and substantially smaller Sn−I−Sn bond angles (152.91° and 152.73°) compared to the unintercalated system, both factors that are correlated with an increase in energy for the optical transitions.[21]

Conclusion

Organic−inorganic perovskites provide a particularly flexible framework in which to tailor properties for potential applications and for the study of interesting physical properties. A number of interactions are responsible for the stabilization of the hybrid perovskites, including ionic and covalent bonding within the inorganic framework, hydrogen bonding and ionic forces between the organic cation and the halides in the inorganic sheets, and weaker van der Waals and aromatic−aromatic interactions among the organic tails of the cations. In this paper, the first two examples of intercalated hybrid perovskites stabilized by fluoroaryl−aryl interaction are reported. Thermal analysis indicates bulk endothermic deintercalation transitions at ∼145 °C for $(C_6F_5C_2H_4NH_3)_2SnI_4 \cdot (C_6H_6)$ and $(C_6H_5C_2H_4NH_3)_2SnI_4 \cdot (C_6F_6)$ crystals, with enthalpies of 12.6(5) and 32.1(8) kJ/mol, respectively. While simple complexes based on the fluoroaryl−aryl interaction typically decompose or melt at relatively low temperature, the robust framework provided by the perovskite layers yields a complex that is stable to temperatures well above 100 °C (although slow deintercalation may take place at lower temperatures), rendering the intercalated perovskites a particularly interesting family in which to consider this important interaction.

Within the hybrid perovskites, the benzene or hexafluorobenzene molecules intercalate at a site sandwiched between the pentafluorophenyl or phenyl rings from adjacent cation layers. Intermolecular C···C interactions in the range 3.44−3.50 Å (smaller than twice the van der Waals radius for aromatic carbon) reflect the substantial face-to-face interaction between the intercalated species and the organic cations. In addition, C−F···H−C contacts (2.6−2.8 Å) between each intercalated molecule and organic cations in neighboring cation/intercalated molecule/cation sandwiches may also contribute to stabilizing the observed structures. The face-to-face stacking and intermolecular interactions are analogous to those observed in the $C_6H_6 \cdot C_6F_6$ complex,[60] suggesting a similar predominantly electrostatic origin to the interaction. Crystal growth runs in which both the prospective intercalating molecule and organic cation are either both fluorinated or both unfluorinated did not result in a stable intercalated hybrid, further highlighting the significance of the fluoroaryl−aryl interaction in these compounds.

The fluoroaryl−aryl-stabilized perovskites provide a new means of tailoring organic−inorganic hybrids for technological or scientific purposes and represent one of the first demonstrations of simple chemistry within the van der Waals gap of the hybrid perovskites. In the current compounds, the intercalated molecule essentially pries the inorganic sheets further apart. The ability to change the separation between the layers enables an examination of the effect of interlayer coupling on the electronic properties of the hybrids. In this study, the optical properties are found to only shift slightly with increasing separation between the inorganic layers (and most of this change can be attributed to structural shifts within the tin iodide sheets as a result of intercalation), thereby demonstrating the predominantly two-dimensional nature of the electronic structure. In addition to affecting interlayer coupling and intralayer bonding, it is expected that intercalating molecules can be chosen to provide charge transfer, photochemical/chemical reactivity, and other interactions between the intercalated species and the organic cations of the perovskite sheets, or among the intercalated species themselves, providing an exciting opportunity to tailor this scientifically and technologically interesting class of materials.

Supporting Information Available: An X-ray crystallographic file, in CIF format, containing information for $(C_6F_5C_2H_4NH_3)_2SnI_4 \cdot (C_6H_6)$ and $(C_6H_5C_2H_4NH_3)_2SnI_4 \cdot (C_6F_6)$. This material is available free of charge via the Internet at http://pubs.acs.org.

IC011190X

(65) Mitzi, D. B. Unpublished work.